Effects of whole body vibration on breast cancer bone metastasis and vascularization in mice

Takeshi Matsumoto[1], Akihiro Mukohara[2]

1. *Tokushima University Graduate School of Technology, Industrial and Social Sciences*
2. *Tokushima University Faculty of Science and Technology*

Corresponding author: Takeshi Matsumoto, PhD
Tokushima University
Graduate School of Technology, Industrial and Social Sciences
2-1 Minamijyousanjima, Tokushima 770-8506, Japan
t.matsumoto@tokushima-u.ac.jp

Abstract

We evaluated whether whole body vibration (WBV) prevented bone loss induced by breast cancer (BC) metastasis and the involvement of bone marrow vasculature. One day after orthotopic transplantation of mammary 4T1 tumor cells, 8-week-old BALB/c mice were subjected to 0.3 *g*/90 Hz vertical vibration for 20 min/day for 5 days/week (BC-WBV) or sham-handled (BC-Sham) over 3 weeks. Age-matched intact mice (Intact) were also sham-handled. Both tibiae were harvested from BC-WBV (n = 7), BC-Sham (n = 9), and Intact (n = 5) mice for bone structure imaging by synchrotron radiation-based computed tomography (SRCT) and hematoxylin and eosin staining, whereas right tibiae were harvested from other BC-WBV and BC-Sham (n = 6 each) mice for vascular imaging by SRCT. Tumor cells were similarly widespread in the marrow in BC-WBV and BC-Sham mice. In BC-Sham mice, cortical bone volume, trabecular volume fraction, trabecular thickness, trabecular number density, and bone mineral density were smaller, and marrow volume and trabecular separation were larger than in Intact mice. However, although trabecular thickness was smaller in BC-WBV than Intact mice, the others did not differ between the two groups. Serum osteocalcin tended to be higher in BC-WBV than BC-Sham mice. Compared with BC-Sham mice, BC-WBV mice had a smaller vessel diameter, a trend of a larger vessel number density, and smaller vessel diameter heterogeneity. In conclusion, WBV mitigates bone loss in BC bone metastasis, which may be partly due to increased bone anabolism. The alteration of marrow vasculature appears to be favorable for anti-tumor drug delivery. Further studies are needed to clarify the multiple actions of WBV on bone, tumor, and marrow vasculature and how they contribute to bone protection in BC metastasis.

Keywords: *exercise, 4T1 tumor cells, metastatic bone loss, tumor vasculature, synchrotron radiation tomography*

Introduction

Breast cancer (BC) is the most frequently diagnosed cancer and the main cause of cancer death in women worldwide [1]. With significant progress in early detection, treatment, and disease management, the survival rate of patients with primary BC has largely improved, especially in high income countries [2]. Nevertheless, once BC metastasizes to distant organs, most patients have a poor prognosis and their quality of life is severely impaired. Bone is the most frequent site of distant involvement of BC because of the high propensity of BC to metastasize to bone [3]. Bone metastases from BC are often accompanied by osteolytic bone destruction that releases bone matrix-derived tumor chemoattractants and growth factors. These factors in turn contribute to metastatic progression, thereby leading to a vicious cycle of bone destruction and cancer growth [4]. Patients with bone-only BC metastasis have a favorable prognosis compared with other metastases in other sites [5]. However, BC bone metastasis remains largely incurable and BC-mediated acute osteolysis followed by bone destruction causes devastating complications, so-called skeletal related events, which include refractory bone pain, pathological fractures, spinal compression, and hypercalcemia [6]. Anti-resorptive drugs prescribed to suppress osteoclast activity, such as bisphosphonates and denosumab, are effective against BC-induced bone loss, but long-term use can lead to osteonecrosis of the jaw and atypical femoral fractures [7]. Safe and effective alternatives to pharmacological intervention to prevent metastatic bone destruction is critical to improve the quality of life of BC patients.

Bone is mechanosensitive and a remodeling balance between bone resorption and formation is maintained to meet the mechanical demands of daily living. Thus, mechanical loading on bone via exercise has been accepted as a low cost and non-pharmacological treatment for patients with osteoporosis or osteopenia [8, 9]. Exercise may also exert a protective effect against metastatic BC-induced bone loss. Epidemiological studies suggest that exercise is efficacious to preserve bone health in BC patients [10, 11]. In a mouse model of BC bone metastasis, moderate loading had an inhibitory effect on bone destruction [12, 13]. Importantly, however, BC cancer patients may have profound difficulty in benefiting from exercise because their bones may already be prone to fracture and fatigue or pain associated with cancer and its treatment interfere with exercise participation [14].

In terms of bone safety and convenience, whole body vibration (WBV) elicits a bone-anabolic response even with low intensity mechanical stimuli [15], which has the potential to serve as a passive exercise effective against cancer-induced bone loss with little risk for bone damage. Generally accepted frequency and magnitude ranges of WBV are 20–100 Hz and <1 g (g = 9.8 m/s^2) or <10 με, respectively. These ranges include those mainly observed in the strain history of bone [16] attributed heavily to postural muscle dynamics [17]. It has been reported that WBV is safely accessible to childhood cancer survivors and protective against bone loss [18]. Another study examined the efficacy of WBV in postmenopausal, bone metastasis-free BC patients receiving aromatase inhibitor therapy although no effect was found on either bone turnover or physical function [19]. In vivo studies in tumor-bearing mice have also shown the effectiveness of WBV against cancer bone metastasis by preserving trabeculae in tibial and vertebral bones

without tumorigenesis acceleration in ovarian cancer metastasis [20] and reducing myeloma burden in bone by deceleration of bone structure deterioration [21].

The response of bone metastasis to WBV may depend on the cancer type. To our knowledge, there has been no study on the protective effect of WBV against bone loss by BC metastasis. Therefore, we investigated the benefits of WBV in suppressing metastatic BC-induced bone loss by employing mice with 4T1 murine mammary tumors. Additionally, we focused on the structure of the bone marrow vasculature in BC metastasis because its abnormality is involved in both the progression of tumor growth and the delivery of anti-tumor drugs [22, 23]. Three-dimensional images of the bone structure and marrow vasculature in BC metastasis with or without WBV treatment were acquired by synchrotron radiation-based computed tomography (SRCT) with vascular casting.

Materials and Methods

The protocol of the animal treatment was in accordance with the guiding principles of the Care and Use of Laboratory Animals of Tokushima University and approved by the Ethics Committee on Animal Experiments of Tokushima University (permit no. T27-111). The synchrotron radiation experiments were performed with the approval of the Japan Synchrotron Radiation Research Institute (proposal nos. 2014B1766, 2015A1922, and 2016A1137).

Animal model and experimental design

The murine BC cell line 4T1 was used to cause metastatic bone loss in mice. The 4T1 cell line, which was generously provided by Prof. Motowo Nakajima (Tokyo University, Tokyo, Japan), was cultured in RPMI-1640 medium with 10% fetal bovine serum and 0.03% kanamycin sulfate at 37°C in a 5% CO_2 humidified incubator. On the day of use, subconfluent 4T1 cells were washed in Dulbecco's phosphate-buffered saline (DPBS) and suspended in DPBS at a density of 1×10^7 cells/mL.

Thirty-seven female BALB/c mice aged at seven weeks were purchased from Japan Charles River (Yokohama, Japan). Mice were housed in a plastic cage under standard conditions (12-h light/dark cycle, 25°C, and 60% humidity) with free access to a standard diet (MF; Oriental Yeast, Tokyo, Japan) and tap water. After a 1-week acclimatization period, 32 mice were anesthetized with isoflurane and injected with 5×10^5 4T1 cells in 50 µl DPBS into the mammary fat pad using a 29-G insulin syringe. The day after 4T1 cell injection (day 0), 4T1-bearing mice were randomly divided into two groups (n = 16 each) treated with WBV (BC-WBV) or sham-treated (BC-Sham). In a pilot study, the present dose of 4T1 cells resulted in significant bone destruction but retained the shape of tibial cortical bone 3 weeks after the injection, which allowed between-group comparisons. The remaining five mice were kept intact and sham-treated (Intact) to provide a baseline to identify the progression of bone loss by this dose of 4T1 cells.

BC-WBV mice underwent 20 minutes/day of vertical sine-wave vibration with a 0.3 *g* amplitude at 90 Hz for 5 days/week. Mice were placed in a compartmented cage that was firmly fixed by screws to a

rigid vibration platform [24]. The platform was driven by an electromagnetic actuator connected to a power supply/amplifier/controller (Big-Wave; Asahi Seisakujo, Tokyo, Japan). Using data received from an accelerometer attached to the platform, the vibration controller generated the input signal, which controlled the gain of the amplifier to produce the required sine-wave vibration. Administration of WBV to BC-WBV mice was performed at around the same time for 3 weeks, and BC-Sham and Intact mice were treated similarly but without vibration exposure.

All mice were kept under standard conditions for 3 weeks until day 21. Body weight was measured after each treatment. One and three mice in BC-Sham and BC-WBV mice, respectively, were euthanized or died between days 16 and 18. These mice were visually examined in the thoracic and abdominal cavities, and extensive and exclusive BC metastasis was found in all the four mice.

Sample preparation

On day 21, Intact (n = 5), BC-Sham (n = 9), and BC-WBV (n = 7) mice were euthanized by an intraperitoneal overdose of pentobarbital sodium. Both tibiae were harvested, dissected from soft tissue, and fixed in 4% paraformaldehyde with the right tibia used for CT scanning and the left tibia for hematoxylin and eosin (H&E) staining. The remaining BC-Sham and BC-WBV mice (n = 6 each) underwent vascular casting as described previously [25]. Briefly, under isoflurane anesthesia, mice were laparotomized, and the left femoral artery and vein were ligated. Following an overdose of pentobarbital sodium for euthanasia, the chest was promptly opened and a 22-G polyethylene catheter was inserted into the left ventricle. The right atrium was cut open to allow fluid to exit and the vascular bed was flushed by injecting 50 mL heparinized saline (37°C, 100 U/ml) and subsequently injecting 5 mL of 0.1 M phosphate buffer (37°C) into the left ventricle. Then, the vascular bed was perfused with a zirconium-based contrast agent (ZrCA) at 120 mmHg and 40°C. This contrast agent was a mixture of 30 mL of 1.2% w/v agarose (Super LM; Nacalai Tesque, Kyoto, Japan) in 0.1 M phosphate buffer and 15 mL of a 62% (w/v) water-based suspension of colloidal zirconium dioxide particles of 0.07–0.1 μm (ZR40BL; Nissan Chemical Industries, Tokyo, Japan). Once perfusion had completed, the abdominal artery and vein were ligated and the entire body was immersed in an ice-cold water bath for approximately 1 h and then stored overnight at 4°C. The right tibia was harvested and fixed in 4% paraformaldehyde until CT scanning.

Imaging by SRCR

The right tibia from each mouse with or without administration of the contrast agent was sealed in a polyethylene tube that contained 4% paraformaldehyde and scanned by SRCT at beamline 20B2 in SPring-8 (Harima, Japan). A visible light conversion type X-ray detector, which consisted of a scientific CMOS camera (C11440-22C; Hamamatsu Photonics, Hamamatsu, Japan) and a beam monitor (BM2; Hamamatsu Photonics) with a 10-μm-thick phosphor screen ($Gd_2O_2S:Tb^+$), was used. Each tibia was scanned with 17.95-keV synchrotron light over an angular range of 0–180° in 0.1° increments with 0.2 s of exposure per

frame. For calibration to compensate for X-ray source instability, 30 images of the X-ray beam alone were recorded at the start and end of each scan. For background correction, 30 dark images were also collected. The scan dataset was reconstructed with a filtered back-projection algorithm provided by SPring-8, which provided a two-dimensional image stack composed of 2.75-μm cubic voxels in 8-bit grayscale. Vascular-casted tibiae were also scanned with 18.05 keV synchrotron lights.

The 17.95 and 18.05 keV images of vascular-casted tibiae were calibrated so that the range of the linear absorption coefficient (μ) of 0–40 cm^{-1} corresponded to the full grayscale range of 0–255. This calibration resulted in substantial enhancement of vascular contrast in 18.05 keV images and similar bone contrast in 17.95- and 18.05-keV images because these energies were just below and above the K-absorption edge of ZrCA. Therefore, selective visualization of vascular structure was possible by subtraction between a pair of 17.05 and 18.05 keV images [25]. Prior to image subtraction, the 17.9 keV image was corrected for misalignment against the 18 keV image by mutual information-based image registration and processed with a 3 × 3 × 3 maximum filter to reduce unwanted residuals near bone boundaries in the subtracted image. The vascular image yielded by image subtraction was filtered by 3 × 3 × 3 voxels averaging and binarized using Otsu's thresholding method.

Bone images for analysis were obtained from the 17.95 keV images both with and without vascular contrast. The grayscale was calibrated to range in μ from 0 to 14 cm^{-1} to increase the resolution of the bone mineral density. The binarized vascular image obtained in advance was subtracted from the image with vascular contrast after similar correction for misalignment, which yielded bone images without vascular regions. One of the benefits of using monochromatic synchrotron light in CT is free of beam hardening artifacts, which is of great advantage in translating the reconstructed image into the distribution of bone mineral density. There was the highly linear relation: $\mu = 7.58 \times \rho + 1.03$ ($r^2 > 0.999$) obtained from the 17.95 keV scan dataset of K_2HPO_4 phantom solutions (0–1 g/mL) and all voxels of $\mu > 4.82$ cm^{-1}, equivalent to the bone mineral density (ρ) > 0.5 g/cm^3, were classified as cortical or cancellous bones.

Quantitative parameters for bone and vascular structures

Structural analysis was carried out in a 1.4-mm-long section of the tibial proximal metaphysis, which began at 0.3 mm distal to the growth plate, providing 510 contiguous slice images. After binarization of the bone images with the threshold value of $\rho = 0.5$ g/cm^3, the bone region was dilated with a kernel size of 3 × 3 voxels. Then, the outer and inner (endocortical) boundaries of cortical bone mask were determined by raster scanning in multiple directions over 0–180° with a step size of 2°. The voxels of $\rho > 0.5$ g/cm^3 within the cortical bone mask were classified as the cortical bone, and the other voxels of $\rho > 0.5$ g/cm^3 were classified as the trabecular bone. The following bone structure parameters were measured: cortical bone thickness (Ct.Th; μm), cortical bone porosity (Ct.P; %), marrow volume (Ma.V; mm^3), trabecular volume fraction (BV/TV; %), trabecular number density (Tb.N; mm^{-3}), mean trabecular thickness (Tb.Th; μm), and mean trabecular separation (Tb.Sp; μm). Calculation of Ct.Th was done after filling all cortical pores. The BoneJ

plugin 1.4.3 for ImageJ 1.53b was used to calculate these parameters [26]. In a similar manner, the structural parameters of marrow vasculature, such as the vessel volume fraction (V.Vf; %), vessel number density (V.N; mm^{-3}), and mean vessel separation (V.Sp; μm) were measured using BoneJ by replacing the images of trabeculae bone with marrow blood vessels. Marrow spaces between vessels and trabeculae as well as between vessels were included to calculate V.Sp. Mean vessel diameter (V.D; μm) and diameter-specific V.Vf were also obtained using a custom C program, where the diameter of each vessel segment was defined as an average of the local vessel diameter over its skeleton line. Additionally, using the linear μ–ρ relation, voxel values were transformed into mineral densities and local values of mineral density were determined for cortical and cancellous bone. Mean mineral density and the mineral density showing the peak of the frequency distribution of mineral density were determined in each specimen.

Histology

The left tibia from mice without administration of the contrast agent was decalcified in a 10% EDTA solution and embedded in paraffin. Serial, longitudinal, 5-μm-thick sagittal sections were cut from each sample. Sections were deparaffinized in xylene, rehydrated in an ethanol gradient, and stained with H&E.

Bone markers

Blood samples were collected from the left ventricle during vascular casting and centrifuged at 1,200 *g* for 20 min. The serum was stored at –80°C until use. Enzyme-linked immunosorbent assays (ELISAs) were employed to determine the serum concentrations of osteocalcin (OC) and tartrate-resistant acid phosphatase 5b (TRACP-5b) as markers of bone formation and resorption, respectively, with an OC EIA kit (Biomedical Technologies Inc, Stoughton, MA, USA) and a TRACP-5b ELISA kit (Immunodiagnostic Systems Inc, Fountain Hills, AZ, USA) in accordance with the manufacturers' protocols.

Statistical analysis

Data are presented as the mean ± SD. Equality of variances and normality of the data frequency distribution were verified by Bartlett's test and the Kolmogorov–Smirnov test, respectively. The two-tailed Kruskal–Wallis test followed by Dunn's multiple comparison test or the two-tailed Mann–Whitney-U test was used to assess between-group differences because the data frequently violated the assumptions of equality of variances between groups or Gaussian distribution. All data were analyzed by Prism 8.2.0 (GraphPad Software; San Diego, CA). $P < 0.05$ was considered statistically significant.

Results

Body weight did not significantly change over time or between groups (Intact, BC-Sham, and BC-WBV mice weighed 19.5 ± 1.2, 19.6 ± 0.6, and 20.2 ± 0.6 g on day 0 and 21.1 ± 1.3, 19.8 ± 0.3, and 20.3 ± 1.9 g on day 21, respectively).

Three-dimensional reconstructions of the proximal tibial metaphysis segmented into cortical and cancellous bone are shown in Figure 1 and bone structural parameters are summarized in Table 1. Osteolytic bone loss in BC-Sham mice was characterized by a smaller Ct.Th, BV/TV, Tb.Th, and Tb.N and a larger Tb.Sp than those in Intact mice, which indicated an increase in structural vulnerability. Cortical bone loss appeared to be prevalent on the endosteal side as implied by the difference between cortical bone images of Intact and BC-Sham mice and the larger Ma.V in BC-Sham mice than in Intact mice. No differences were found in bone structural indices between Intact and BC-WBV mice except for Tb.Th that was smaller in BC-WBV mice. Compared with BC-Sham mice, BC-WBV mice had a larger Ct.Th and Tb.N, a smaller Ma.V and Tb.Sp, and a tendency of a higher BV/TV (P = 0.09), which indicated the bone-protective potential of WBV.

Figure 2 compares the frequency distributions of mineral density (relative number of voxels at each mineral density) in cortical and cancellous bones of the proximal tibial metaphysis between the three groups. For cortical bone, the distribution in BC-WBV mice showed an intermediate profile between Intact and BC-Sham mice. Mean mineral density in BC-Sham mice (1.13 ± 0.02 g/cm^3) was significantly smaller than that in BC-WBV (1.18 ± 0.02 g/cm^3, $P < 0.01$) and Intact (1.26 ± 0.03 g/cm^3, $P < 0.0001$) mice. The peak frequencies were located at 1.39 ± 0.04, 1.24 ± 0.03, and 1.31 ± 0.03 g/cm^3 in Intact, BC-Sham, and BC-WBV mice, respectively. The mineral density with the peak frequency was significantly lower in BC-Sham mice than in BC-WBV ($P < 0.05$) and Intact ($P < 0.0001$) mice. For the cancellous bone, the mean mineral density in BC-Sham mice (0.93 ± 0.01 g/cm^3) was significantly smaller than that in BC-WBV (0.95 ± 0.01 g/cm^3, $P < 0.05$) and Intact (1.01 ± 0.03 g/cm^3, $P < 0.0001$) mice. However, the distributions in BC-Sham and BC-WBV mice were similar with peaks at 1.07 ± 0.01 and 1.08 ± 0.02 g/cm^3, respectively. These values were significantly smaller ($P < 0.05$ and $P < 0.0005$, respectively) than the mineral density with the peak frequency (1.16 ± 0.04 g/cm^3) of the distribution in Intact mice.

The marrow vasculature and trabeculae of BC-Sham and BC-WBV mice are shown in three-dimensional reconstructions in Figure 3. Saccular vessels were found frequently in BC-Sham mice, but not as frequently in BC-WBV mice. Figure 4 shows the diameter-specific V.Vf for 14 diameter ranges with mean ± SD values of V.Vf, V.N, V.Sp, and V.D in each group. On average, BC-WBV mice had a smaller V.D and V.Sp, and a trend of a larger V.N (P = 0.06) than BC-Sham mice. Both groups showed a monomodal distribution of diameter-specific V.Vf, which peaked in the range of 16.5–22.0 μm. However, V.Vf was higher in the range of 11.0–16.5 μm and tended to be higher in the range of 16.5–22.0 μm (P = 0.09) in BC-WBV mice than in BC-Sham mice. Conversely, V.Vf was smaller in the ranges of 44.0–60.5, 66.0–71.5, and >77.0 μm, and tended to be smaller in the range of 60.5–66.0 μm (P = 0.06) in BC-WBV mice than in BC-Sham mice. Therefore, the heterogeneity of the marrow vessel diameter was smaller in BC-WBV mice.

Histological H&E-stained sagittal sections of proximal tibial bone are shown in Figure 5 for Intact, BC-Sham, and BC-WBV mice. In both 4T1-bearing groups, the metastatic lesion had infiltrated

throughout much of the marrow cavity and replaced most of the normal marrow tissue. All tibial bone sections similarly had widespread tumor cells with or without WBV exposure.

The serum levels of OC and TRACP-5b were 68 ± 22 ng/mL and 7.3 ± 0.9 U/L, respectively, in BC-Sham mice and 91 ± 27 ng/mL and 7.3 ± 1.6 U/L, respectively, in BC-WBV mice. Although neither of these bone markers differed between the two groups, OC tended to be higher in BC-WBV mice ($P = 0.056$).

Discussion

In the present study, we showed the effectiveness of WBV to slow the progression of metastatic bone loss in 4T1 murine BC-bearing mice. The 3-week WBV exposure did not halt metastatic tumor progression, but alleviated deterioration of the bone structure and reduced the decline in cortical bone mineralization. In addition to its positive effect on bone structure, WBV lowered and elevated the proportions of large- and small-diameter vessels, respectively, thereby decreasing both the mean diameter and diameter heterogeneity of bone marrow vasculature.

There have been few studies on the effects of WBV on bone loss associated with cancer metastasis. A prospective randomized clinical trial reported the benefit of WBV to prevent or reverse a decline in the bone mineral density in pediatric cancer survivors [18], and in murine models of ovarian cancer and myeloma, WBV alleviated metastatic bone loss [20, 21]. It has also been reported that WBV had no effect on bone turnover in BC patients who received aromatase inhibitor therapy but had no bone metastases [19]. This study first investigated whether WBV is effective against bone loss and structural deterioration in BC bone metastasis. The high resolution quantitative CT using monochromatic synchrotron light demonstrated its positive effects against metastatic bone loss in mice injected with 4T1 tumor cells into the mammary fat pad. The 3-week WBV exposure in tumor-bearing mice diminished the decreases of the cortical bone thickness and mineral density, the reduction of the trabecular volume ratio, and the increases of the trabecular space and marrow volume. Although metastatic BC-induced bone loss was observed in mice treated with WBV, its bone-protective action made the BC-metastasized bone comparable in terms of structural indices, except for trabecular bone thickness, with healthy bone at least statistically.

Bones are exposed to high and low strains via numerous mechanical loads in daily life and low strains of < 10 με occur thousands of times daily [16]. Mechanical vibrations of WBV safely propagate to bone tissue wherein low strains and high frequency accelerations arise, causing a cellular osteogenic response [27-29]. The osteogenic capacity of osteoblasts and bone marrow-derived mesenchymal stem cells (MSCs) has been reported to increase in response to low magnitude, high-frequency vibration (LMHFV) [30, 31]. The bone-protective effect of WBV was observed in spinal cord-injured rats and type-2 diabetic mice [32, 33]. This effect occurred at least partly through the bone anabolic action, as indicated by elevated serum levels of OC. Our study also showed a tendency for higher serum OC levels in BC-WBV mice than in BC-Sham mice, which indicated the contribution of the bone-anabolic action induced by WBV to alleviate metastatic BC-induced bone loss.

On the other hand, the anti-osteolytic action of WBV could not be recognized from serum TRACP-5b levels in BC-WBV and BC-Sham mice. However, as responses to LMHFV, there have been reported that osteoblasts and bone marrow-derived MSCs suppress osteoblast-mediated osteoclastogenesis via the ERK1/2 pathway [34, 35] and that osteocytes and osteoclasts may act suppressively against osteoclast formation and differentiation [36, 37]. In fact, the anti-osteolytic action of WBV accompanying decreased serum levels of TRACP-5b has been observed in murine models of myeloma and type 2 diabetes [21, 33]. A possible reason for no effect of WBV on serum TRACP-5b levels is that WBV cannot counteract the osteolytic activity mediated by highly malignant 4T1 tumor cells, as implied by a confluent tumor burden, which was similarly observed in BC-WBV and BC-Sham mice (Fig. 5). Alternatively, it remains possible that the expression of bone resorption markers differs significantly between BC-WBV and BC-Sham mice within the metastatic bone lesion. The local activities of osteoclasts, as well as osteoblasts and tumor cells, will be worth investigating in future studies.

Recent in vitro studies have demonstrated that exposure of MDA-MB-231 BC cells to LMHFV decreases their aggressive behaviors such as invasive and proliferative capacities [38, 39], which suggests that WBV is also helpful to suppress tumor growth in BC bone metastasis. However, in our study with 4T1-bearing mice, WBV, although effective against tibial bone destruction, did not suppress the metastatic spread of 4T1 cells over the marrow cavity of the tibial bone (Fig. 5). We used the murine syngeneic model of metastatic BC, in which 5×10^5 4T1 tumor cells were transplanted into the mammary fat pad. 4T1 is a triple-negative BC cell line that exhibits a high degree of malignancy and highly preferential metastasis to bone. Thus, the failure of WBV to protect against the widespread growth of 4T1 tumor cells in the tibial compartment may have occurred because mechanical signals derived from WBV could not outpace the aggressive malignant activity of metastatic 4T1 tumor cells. Therefore, 4T1 mammary tumor cells characterized by high degrees of aggressiveness and bone preference may have a limited observation window to determine whether WBV is beneficial to counteract the progression of bone metastatic tumor growth. Multiple timepoint observations, which include early time points, are needed to clarify the protective effect of WBV against bone tumor growth in the present murine model of BC bone metastasis.

Solid tumor vasculature is characterized by irregular vessel arrangements with a distorted shape and heterogeneity in the vessel diameter. In BC metastatic bone lesions, tumor vasculature is also heterogeneous, which is attributed to the appearance of large-diameter vessels and the reduction in small-diameter vessels [40, 41]. It has been further reported that according to the tumor progression in BC bone metastasis, vessel diameter heterogeneity of tumor vasculature increases, and vessel frequency distribution shifts toward higher vessel diameters [40]. Thus, the diameter-specific vascular volume fraction and the mean vessel diameter in BC-Sham mice (Fig. 4) should have shown the feature of tumor vasculature in the metaphyseal bone marrow, to which 4T1 tumor cells metastasized entirely (Fig. 5).

Heterogeneous vasculature in solid tumors causes not only low perfusion, but also heterogeneous perfusion, which may lead to regional tissue hypoxia [42, 43]. Hypoxia confers tumors with aggressive and

metastatic phenotypes, and heterogeneous perfusion coupled with increased interstitial fluid pressure invokes inefficient delivery of anti-tumor drugs in low-perfused tumor regions [44-46]. Therefore, normalizing tumor vasculature and thus improving tumor perfusion and oxygenation is effective against tumor growth as well as the poor distribution of anti-tumor drugs [22, 23]. Bone marrow vessels in BC-WBV mice were comparable in terms of diameter distribution with those previously observed in BC metastatic bone lesions at a very early stage [40], where the distribution of vessel diameters peaks at around 10–20 μm and maintains a certain degree of uniformity. Thus, WBV may contribute to reducing diameter heterogeneity of tumor vasculature and shifting the vessel frequency distribution toward smaller vessel diameters in BC bone metastasis. Such changes in tumor vasculature, which are the opposite of those that accompany the tumor progression in BC bone metastasis [40], could reduce the degree of perfusion heterogeneity. Furthermore, the trend of the high vessel density in the metastasized marrow of BC-WBV mice, where small-diameter vessels comprised the majority, could lead to the perfusion increase. In this respect, although this study demonstrated only the benefit of WBV against metastatic bone loss, it may also be effective against bone metastatic tumor growth, especially in combination with anti-tumor drugs. The mechanisms of WBV in modifying the vessel diameter distribution of tumor vasculature are beyond the scope of this study. However, they will involve a balance of pro- and anti-angiogenic factors [22]. Additionally, it is possible that the WBV-induced remission of interstitial hypertension, which would relieve the compression of tumor vessels and allow collapsed vessels to reopen [44], might contribute to increasing the number of small-diameter vessels to be filled with the contrast agent. To evaluate the benefits of WBV in BC-metastasized marrow perfusion, further studies are needed on whether WBV is effective against tumor vessel leakiness and interstitial hypertension.

There are several limitations, other than those already discussed, in this study. First, we assessed BC bone metastasis only in the tibial bone. The benefits of WBV against BC might also be present in the primary tumor site of mammary fat. In a study of mammary BC tumor-bearing mice [47], knee loading induced alteration in systemic metabolites such as cholesterol and calcitonin, thereby reducing Wnt1-inducible signaling pathway protein 1 (WISP1), which as a result, remotely suppressed the mammary tumor growth. The same study also found a reduced urinary level of WISP1 in humans in response to step aerobics. Thus, the benefit of WBV to alleviate metastatic BC-induced bone loss is possibly attributed partly to its effect mediated via circulatory factors against the primary tumor site. Although this study does not indicate an effect of WBV on the primary tumor site because the numbers of mice that died of BC lung metastasis was one in the BC-Sham group, but three in the BC-WBV group, further study is needed to determine whether the anti-tumor action of WBV is effective even at a distance. Furthermore, the degree of the benefit from WBV may vary between skeletal sites, and it is difficult to extrapolate the present results to other skeletal sites, such as the proximal femur and spine, which are most likely to suffer cancer metastasis. For example, in myeloma-induced mice, WBV was more bone-protective in the femoral bone than in the tibial bone, which suggests a relationship to between-bone differences in the marrow volume or in mechano-

responsivity of marrow-derived MSCs [21, 48]. Distance from the vibration plate may also influence the skeletal response to WBV. In general, the farther from the plate, the magnitude of tissue strain or acceleration induced by WBV is thought to become smaller. However, the effect of WBV on bone is not necessarily smaller. For instance, WBV at 45 Hz can be more effective in increasing trabecular bone volume in mice when the amplitude is 0.1 *g* than 0.3 *g* [49]. Second, we lacked data on the effective regimen of WBV treatment. In the two earlier animal studies that investigated the benefits of WBV against cancer-induced bone loss [19, 20], mice were administered a vibratory signal of 90 Hz at 0.3 *g* for 15 min/day for 5 days/week. We followed this loading regimen except for the daily administration time, which was altered to 20 min. Numerous studies, which include these two animal studies, have demonstrated that the effect of WBV at this frequency and intensity is bone anabolic, which is expected to be the case in this study. However, it has recently been reported that insertion of non-loaded rest periods between vibration bouts may alleviate desensitization of bone in response to mechanical stimuli and enhance the efficacy of WBV [50]. To increase the effectiveness of a WBV regimen against BC bone metastasis, the effective combination of duration of vibration bouts and between-bout interval in addition to the vibration frequency and intensity needs to be investigated further. Finally, this study was observational and did not provide insights into the detailed mechanisms responsible for the effectiveness of WBV against metastatic BC-induced bone loss. Further studies, including experiments on intact mice, are needed for elucidating how WBV affects bone, tumor, and marrow vasculature and how they are involved in bone protection in BC metastasis.

In summary, 3 weeks of WBV treatment in mammary BC tumor-bearing mice mitigated metastatic bone loss, which may be associated at least partly with its bone-anabolic effect. Further, the reduced heterogeneity of the marrow vessel diameter, accompanied by a shift in vessel distribution toward smaller vessel diameters, was observed in the WBV-treated mice. Such structural changes in tumor vasculature indicated the potential of WBV to reduce tumor progression and improve drug delivery to targeted tumor cells by improving local perfusion. Further studies are required to extrapolate the present findings to patients with BC bone metastasis. The anti-tumor growth and -bone loss effects of WBV starting at different stages of BC bone metastasis or effects depending on metastatic BC tumor cells with various aggressiveness should be examined. Optimizing a WBV protocol that achieves high efficacy, such as by inserting non-loaded rest periods between vibration bouts, is difficult, but crucial for the successful application of WBV as a non-pharmacological treatment for BC bone metastasis.

Acknowledgments

The authors are indebted to Shinya Itamochi (Osaka University Graduate School of Engineering Science) for his assistance with animal experiments and SRCT imaging and to Dr. Takashi Fukushima (Saitama Medical University International Medical Center) for his help in the interpretation of the histological data. We would also like to thank Mitchell Arico from Edanz (https://jp.edanz.com/ac) for editing a draft of this manuscript.

Funding

A part of this study was supported by Japan Society for the Promotion of Science Grant-in-Aid for Scientific Research (nos. 26282120, 15K12509, and 20K21899).

Statements and Declarations

Conflict of interest

The authors declare that they have no conflicts of interest.

Ethical Approval

All animal experiments were approved by the Ethics Committee on Animal Experiments of Tokushima University.

Human and Animal Rights

All animals involved in the study were cared for in accordance with the Declaration of Helsinki. The protocol of animal treatment was in accordance with the guiding principles of the Care and Use of Laboratory Animals of Tokushima University.

References

1. Bray F, Ferlay J, Soerjomataram I, Siegel RL, Torre LA, Jemal A (2018) Global cancer statistics 2018: GLOBOCAN estimates of incidence and mortality worldwide for 36 cancers in 185 countries. CA Cancer J Clin 68:394-424. https://doi.org/10.3322/caac.21492.
2. Cardoso F, Spence D, Mertz S, Corneliussen-James D, Sabelko K, Gralow J, Cardoso MJ et al (2018) Global analysis of advanced/metastatic breast cancer: Decade report (2005-2015). Breast 39:131-138. https://doi.org/10.1016/j.breast.2018.03.002.
3. Chen YC, Sosnoski DM, Mastro AM (2010) Breast cancer metastasis to the bone: mechanisms of bone loss. Breast Cancer Res 12:215. https://doi.org/10.1186/bcr2781.
4. Weilbaecher KN, Guise TA, McCauley LK (2011) Cancer to bone: a fatal attraction. Nat Rev Cancer 11:411-425. https://doi.org/10.1038/nrc3055.
5. Ryan C, Stoltzfus KC, Horn S, Chen H, Louie AV, Lehrer EJ, Trifiletti DM et al (2020) Epidemiology of bone metastases. Bone:115783. https://doi.org/10.1016/j.bone.2020.115783.
6. Oster G, Lamerato L, Glass AG, Richert-Boe KE, Lopez A, Chung K, Richhariya A et al (2013) Natural history of skeletal-related events in patients with breast, lung, or prostate cancer and metastases to bone: a 15-year study in two large US health systems. Support Care Cancer 21:3279-3286. https://doi.org/10.1007/s00520-013-1887-3.
7. Jara MA, Varghese J, Hu MI (2021) Adverse events associated with bone-directed therapies in patients with cancer. Bone:115901. https://doi.org/10.1016/j.bone.2021.115901.
8. Hong AR, Kim SW (2018) Effects of resistance exercise on bone health. Endocrinol Metab 33:435-444. https://doi.org/10.3803/EnM.2018.33.4.435.
9. Zhang S, Huang X, Zhao X, Li B, Cai Y, Liang X, Wan Q (2021) Effect of exercise on bone mineral density among patients with osteoporosis and osteopenia: a systematic review and network meta-analysis. J Clin Nurs. https://doi.org/10.1111/jocn.16101.
10. Fornusek CP, Kilbreath SL (2017) Exercise for improving bone health in women treated for stages I-III breast cancer: a systematic review and meta-analyses. J Cancer Surviv 11:525-541. https://doi.org/10.1007/s11764-017-0622-3.
11. Singh B, Toohey K (2022) The effect of exercise for improving bone health in cancer survivors - a systematic review and meta-analysis. J Sci Med Sport 25:31-40. https://doi.org/10.1016/j.jsams.2021.08.008.
12. Fan Y, Jalali A, Chen A, Zhao X, Liu S, Teli M, Guo Y et al (2020) Skeletal loading regulates breast cancer-associated osteolysis in a loading intensity-dependent fashion. Bone Res 8:9. https://doi.org/10.1038/s41413-020-0083-6.
13. Wang S, Pei S, Wasi M, Parajuli A, Yee A, You L, Wang L (2021) Moderate tibial loading and treadmill running, but not overloading, protect adult murine bone from destruction by metastasized breast cancer. Bone 153:116100. https://doi.org/10.1016/j.bone.2021.116100.

14. Husebø AM, Dyrstad SM, Søreide JA, Bru E (2013) Predicting exercise adherence in cancer patients and survivors: a systematic review and meta-analysis of motivational and behavioural factors. J Clin Nurs 22:4-21. https://doi.org/10.1111/j.1365-2702.2012.04322.x
15. Rubin C, Turner AS, Bain S, Mallinckrodt C, McLeod K (2001) Anabolism. Low mechanical signals strengthen long bones. Nature 412:603-604. https://doi.org/10.1038/35088122.
16. Fritton SP, McLeod KJ, Rubin CT (2000) Quantifying the strain history of bone: spatial uniformity and self-similarity of low-magnitude strains. J Biomech 33:317-325. https://doi.org/10.1016/S0021-9290(99)00210-9.
17. Huang RP, Rubin CT, McLeod KJ (1999) Changes in postural muscle dynamics as a function of age. J Gerontol A Biol Sci Med Sci 54:B352-B357. https://doi.org/10.1093/gerona/54.8.B352.
18. Mogil RJ, Kaste SC, Ferry RJ Jr, Hudson MM, Mulrooney DA, Howell CR, Partin RE et al (2016) Effect of low-magnitude, high-frequency mechanical stimulation on BMD among young childhood cancer survivors: a randomized clinical trial. JAMA Oncol 2:908-914. https://doi.org/10.1001/jamaoncol.2015.6557.
19. Baker MK, Peddle-McIntyre CJ, Galvão DA, Hunt C, Spry N, Newton RU (2018) Whole Body Vibration Exposure on Markers of Bone Turnover, Body Composition, and Physical Functioning in Breast Cancer Patients Receiving Aromatase Inhibitor Therapy: A Randomized Controlled Trial. Integr Cancer Ther 17:968-978. https://doi: 10.1177/1534735418781489.
20. Pagnotti GM, Adler BJ, Green DE, Chan ME, Frechette DM, Shroyer KR, Beamer WG et al (2012) Low magnitude mechanical signals mitigate osteopenia without compromising longevity in an aged murine model of spontaneous granulosa cell ovarian cancer. Bone 51:570-577. https://doi.org/10.1016/j.bone.2012.05.004.
21. Pagnotti GM, Chan ME, Adler BJ, Shroyer KR, Rubin J, Bain SD, Rubin CT (2016) Low intensity vibration mitigates tumor progression and protects bone quantity and quality in a murine model of myeloma. Bone 90:69-79. https://doi.org/10.1016/j.bone.2016.05.014.
22. Goel S, Duda DG, Xu L, Munn LL, Boucher Y, Fukumura D, Jain RK (2011) Normalization of the vasculature for treatment of cancer and other diseases. Physiol Rev 91:1071-1121. https://doi.org/10.1152/physrev.00038.2010.
23. Lugano R, Ramachandran M, Dimberg A (2020) Tumor angiogenesis: causes, consequences, challenges and opportunities. Cell Mol Life Sci 77:1745-1770. https://doi.org/10.1007/s00018-019-03351-7.
24. Matsumoto T, Itamochi S, Hashimoto Y (2016) Effect of concurrent use of whole-body vibration and parathyroid hormone on bone structure and material properties of ovariectomized mice. Calcif Tissue Int 98:520-529. https://doi.org/10.1007/s00223-015-0104-4.
25. Matsumoto T, Goto D, Sato S (2013) Subtraction micro-computed tomography of angiogenesis and osteogenesis during bone repair using synchrotron radiation with a novel contrast agent. Lab Invest

93:1054-1063. https://doi.org/10.1038/labinvest.2013.87.

26. Doube M, Kłosowski MM, Arganda-Carreras I, Cordelières FP, Dougherty RP, Jackson JS, Schmid B et al (2010) BoneJ: free and extensible bone image analysis in ImageJ. Bone 47:1076-1079. https://doi.org/10.1016/j.bone.2010.08.023.
27. Birks S, Uzer G (2021) At the nuclear envelope of bone mechanobiology. Bone 151:116023. https://doi.org/10.1016/j.bone.2021.116023.
28. Uzer G, Thompson WR, Sen B, Xie Z, Yen SS, Miller S, Bas G et al (2015) Cell mechanosensitivity to extremely low-magnitude signals is enabled by a LINCed nucleus. Stem Cells 33:2063-2076. https://doi.org/10.1002/stem.2004.
29. Robinson JA, Chatterjee-Kishore M, Yaworsky PJ, Cullen DM, Zhao W, Li C, Kharode Y et al (2006) Wnt/beta-catenin signaling is a normal physiological response to mechanical loading in bone. J Biol Chem 281:31720-31728. https://doi.org/10.1016/S0021-9258(19)84086-3.
30. Gao H, Zhai M, Wang P, Zhang X, Cai J, Chen X, Shen G et al (2017) Low-level mechanical vibration enhances osteoblastogenesis via a canonical Wnt signaling-associated mechanism. Mol Med Rep 16:317-324. https://doi.org/10.3892/mmr.2017.6608.
31. Lu Y, Zhao Q, Liu Y, Zhang L, Li D, Zhu Z, Gan X et al (2018) Vibration loading promotes osteogenic differentiation of bone marrow-derived mesenchymal stem cells via p38 MAPK signaling pathway. J Biomech 71:67-75. https://doi.org/10.1016/j.jbiomech.2018.01.039.
32. Minematsu A, Nishii Y, Imagita H, Takeshita D, Sakata S (2016) Whole-body vibration can attenuate the deterioration of bone mass and trabecular bone microstructure in rats with spinal cord injury. Spinal Cord 54:597-603. https://doi.org/10.1038/sc.2015.220.
33. Jing D, Luo E, Cai J, Tong S, Zhai M, Shen G, Wang X et al (2016) Mechanical vibration mitigates the decrease of bone quantity and bone quality of leptin receptor-deficient db/db mice by promoting bone formation and inhibiting bone resorption. J Bone Miner Res 31:1713-1724. https://doi.org/10.1002/jbmr.2837.
34. Zhou Y, Guan X, Liu T, Wang X, Yu M, Yang G, Wang H (2015) Whole body vibration improves osseointegration by up-regulating osteoblastic activity but down-regulating osteoblast-mediated osteoclastogenesis via ERK1/2 pathway. Bone 71:17-24. https://doi.org/10.1016/j.bone.2014.09.026.
35. Zhou Y, Guan X, Zhu Z, Gao S, Zhang C, Li C, Zhou K et al (2011) Osteogenic differentiation of bone marrow-derived mesenchymal stromal cells on bone-derived scaffolds: effect of microvibration and role of ERK1/2 activation. Eur Cell Mater 22:12-25. https://doi.org/10.22203/ecm.v022a02.
36. Lau E, Al-Dujaili S, Guenther A, Liu D, Wang L, You L (2010) Effect of low-magnitude, high-frequency vibration on osteocytes in the regulation of osteoclasts. Bone 46:1508-1515. https://doi.org/10.1016/j.bone.2010.02.031.
37. Wu SH, Zhong ZM, Chen JT (2012) Low-magnitude high-frequency vibration inhibits RANKL-induced osteoclast differentiation of RAW264.7 cells. Int J Med Sci 9:801-807.

https://www.medsci.org/v09p0801.htm.

38. Olcum M, Ozcivici E (2014) Daily application of low magnitude mechanical stimulus inhibits the growth of MDA-MB-231 breast cancer cells in vitro. Cancer Cell Int 14:102. https://doi.org/10.1186/s12935-014-0102-z.
39. Yi X, Wright LE, Pagnotti GM, Uzer G, Powell KM, Wallace JM, Sankar U et al (2020) Mechanical suppression of breast cancer cell invasion and paracrine signaling to osteoclasts requires nucleo-cytoskeletal connectivity. Bone Res 8:40. https://doi.org/10.1038/s41413-020-00111-3.
40. Fuhrhop I, Schroeder M, Rafnsdóttir SL, Viezens L, Rüther W, Hansen-Algenstaedt N, Schaefer C (2010) Dynamics of microvascular remodelling during tumor growth in bone. J Orthop Res 28:27-31. https://doi.org/10.1002/jor.20968.
41. Nyangoga H, Mercier P, Libouban H, Baslé MF, Chappard D (2011) Three-dimensional characterization of the vascular bed in bone metastasis of the rat by microcomputed tomography (MicroCT). PLoS One 6:e17336. https://doi.org/10.1371/journal.pone.0017336.
42. Grimes DR, Kannan P, Warren DR, Markelc B, Bates R, Muschel R, Partridge M (2016) Estimating oxygen distribution from vasculature in three dimensional tumor tissue. J R Soc Interface 13:20160070. https://doi.org/10.1098/rsif.2016.0070.
43. Bernabeu MO, Köry J, Grogan JA, Markelc B, Beardo A, d'Avezac M, Enjalbert R et al (2020) Abnormal morphology biases hematocrit distribution in tumor vasculature and contributes to heterogeneity in tissue oxygenation. Proc Natl Acad Sci USA 117:27811-27819. https://doi.org/10.1073/pnas.2007770117.
44. Padera TP, Stoll BR, Tooredman JB, Capen D, di Tomaso, E, Jain RK (2004) Cancer cells compress intratumour vessels. Nature 427:695. https://doi.org/10.1038/427695a.
45. Bertout JA, Patel SA, Simon MC (2008) The impact of O_2 availability on human cancer. Nat Rev Canc 8:967-975. https://doi.org/10.1038/nrc2540.
46. Ribatti D, Annese T, Ruggieri S, Tamma R, Crivellato E (2019) Limitations of Anti-Angiogenic Treatment of Tumors. Transl Oncol 12:981-986. https://doi.org/10.1016/j.tranon.2019.04.022.
47. Liu S, Wu D, Sun X, Fan Y, Zha R, Jalali A, Teli M et al (2020) Mechanical stimulations can inhibit local and remote tumor progression by downregulating WISP1. FASEB J 34:12847-12859. https://doi.org/10.1096/fj.202000713RR.
48. Wallace IJ, Pagnotti GM, Rubin-Sigler J, Naeher M, Copes LE, Judex S, Rubin CT et al (2015) Focal enhancement of the skeleton to exercise correlates with responsivity of bone marrow mesenchymal stem cells rather than peak external forces. J Exp Biol 218:3002-3009. https://doi.org/10.1242/jeb.118729.
49. Christiansen BA, Silva MJ (2006) The effect of varying magnitudes of whole-body vibration on several skeletal sites in mice. Ann Biomed Eng 34:1149-1156. https://doi.org/10.1007/s10439-006-9133-5.

50. Gao J, Gong H, Huang X, Zhang R, Ma R, Zhu D (2016) Multi-level assessment of fracture calluses in rats subjected to low-magnitude high-frequency vibration with different rest periods. Ann Biomed Eng 44:2489-2504. https://doi.org/10.1007/s10439-015-1532-z.

Table 1 Bone parameters

	Intact	BC-Sham	BC-WBV
Ct.Th [μm]	180.0 ± 4.0	99.8 ± 4.6$^{\#\#}$	117.2 ± 9.5*
Ct.P [%]	0.68 ± 0.13	0.74 ± 0.15	0.76 ± 0.08
Ma.V [mm^3]	1.54 ± 0.19	2.53 ± 0.20$^{\#\#}$	2.03 ± 0.21*
BV/TV [%]	6.82 ± 0.58	3.80 ± 0.46$^{\#\#}$	4.88 ± 0.55
Tb.Th [μm]	45.0 ± 0.8	33.3 ± 1.3$^{\#}$	33.5 ± 2.1$^{\#}$
Tb.Sp [μm]	281.7 ± 14.3	339.5 ± 34.8$^{\#}$	288.3 ± 18.4*
Tb.N [mm^{-3}]	1688 ± 272	1179 ± 195$^{\#}$	1575 ± 203*

*$P < 0.05$ vs. BC-Sham, $^{\#}P < 0.05$, $^{\#\#}P < 0.01$ vs. Intact.

Figure captions

Figure 1. Examples of cortical and cancellous bone images (mineral density > 0.5 g/cm^3) of the proximal tibial metaphysis reconstructed from Intact, BC-Sham, and BC-WBV mice. The lengths of the orthogonal thick line segments are all 0.5 mm.

Figure 2. Relative volume distributions versus mineral density in cortical (top) and cancellous (bottom) bones of proximal metaphyseal tibiae. The relative volume at each mineral density (bin width: 0.022 g/cm^3) is expressed as a percentage of the total volume of voxels with mineral density > 0.5 g/cm^3. In the cortical bone, the mean mineral density in BC-Sham mice was smaller than that in BC-WBV ($P < 0.01$) and Intact mice ($P < 0.0001$). The mineral density with the peak frequency was lower in BC-Sham mice than in BC-WBV ($P < 0.05$) and Intact ($P < 0.0001$) mice. In the cancellous bone, the frequency distribution peaked at a higher mineral density in Intact mice than in BC-WBV mice ($P < 0.05$) and BC-Sham mice ($P < 0.0005$). Mineral density distributions were similar between BC-Sham and BC-WBV mice, but the mean mineral density was smaller in BC-Sham mice than in BC-WBV mice ($P < 0.05$) and Intact mice ($P < 0.0001$). Error bars are ± standard deviation.

Figure 3. Blood vessels (red) and trabeculae (grey) in the medullary region (yellow) of proximal metaphyseal tibiae of BC-Sham and BC-WBV tumor-bearing mice. Saccular vessels (☆) were more frequently observed in BC-Sham mice. The lengths of orthogonal thick line segments are all 0.5 mm.

Figure 4. Boxplot of the diameter-specific vascular volume fraction in proximal metaphyseal tibiae of BC-Sham and BC-WBV tumor-bearing mice. V.Vf: vascular volume fraction; V.N: vessel number density; V.Sp: mean vessel separation; V.D: mean vascular diameter. *P<0.05, **P<0.01 vs. BC-Sham.

Figure 5. Representative images of H&E staining of tibial sagittal sections from Intact, BC-Sham, and BC-WBV mice. The right panels show enlarged views of the boxed areas (120 × 90 μm) in the left panels. In both BC-Sham and BC-WBV mice, 4T1 tumor cells, which are generally larger than normal bone marrow cells, were widely distributed throughout the bone marrow region. A small number of normal bone marrow cells were also observed to be sparsely scattered, but there were no normal bone marrow compartments.

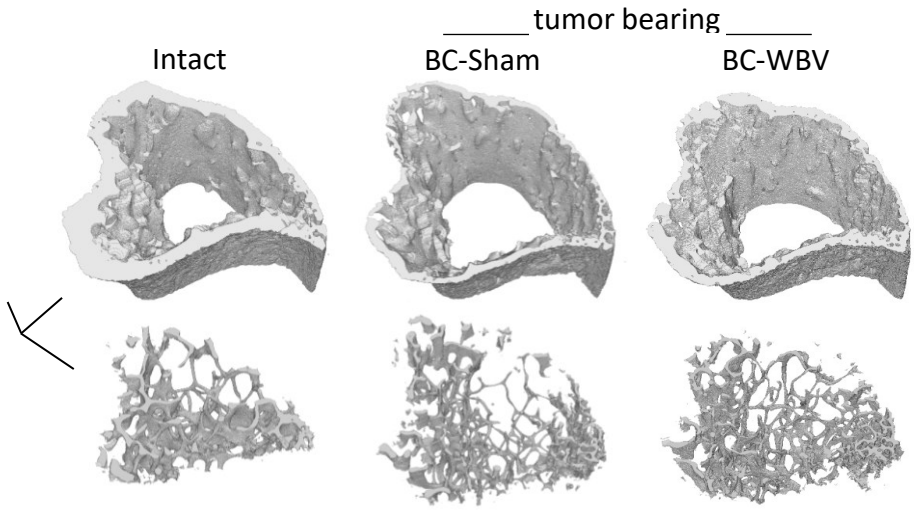

Figure 1

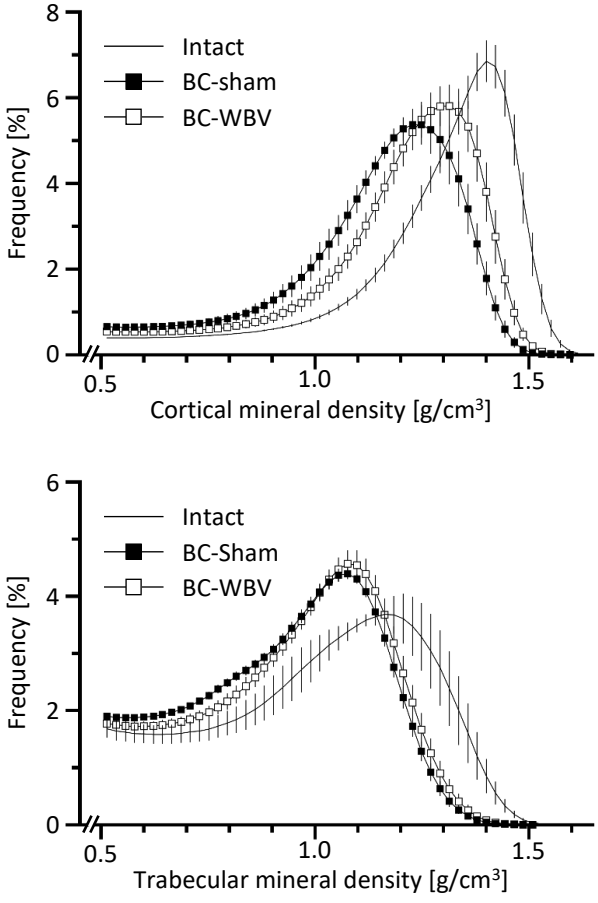
Intact
BC-sham
BC-WBV
Frequency [%]
Cortical mineral density [g/cm³]
Intact
BC-Sham
BC-WBV
Frequency [%]
Trabecular mineral density [g/cm³]

Figure 2

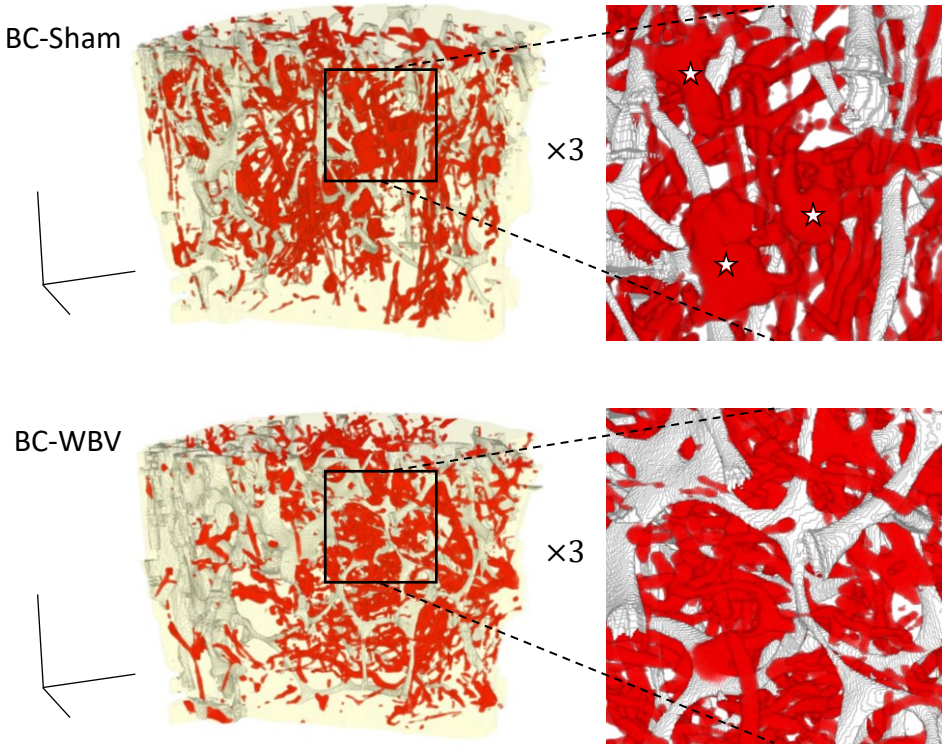

Figure 3

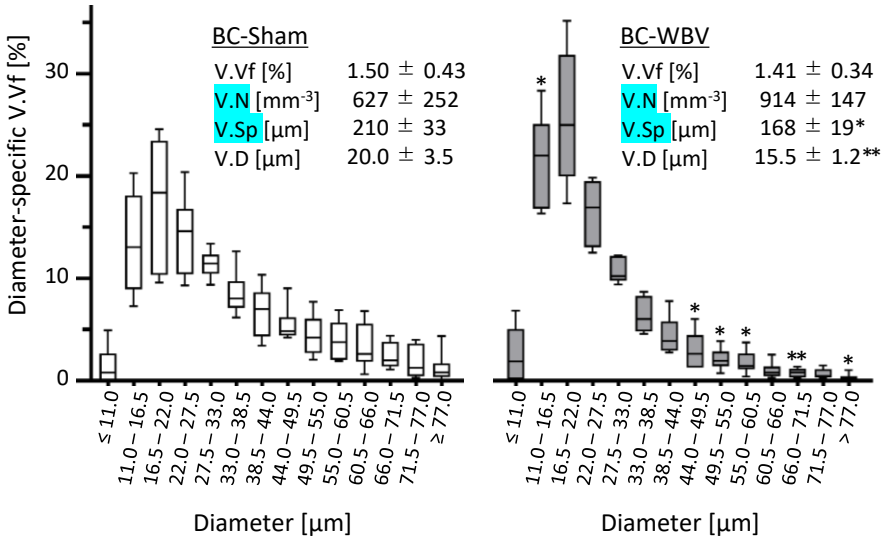
Diameter-specific V.Vf [%]
30
20
10
0
BC-Sham
V.Vf [%] 1.50 ± 0.43
V.N [mm-3] 627 ± 252
V.Sp [µm] 210 ± 33
V.D [µm] 20.0 ± 3.5
BC-WBV
V.Vf [%] 1.41 ± 0.34
V.N [mm-3] 914 ± 147
V.Sp [µm] 168 ± 19*
V.D [µm] 15.5 ± 1.2**
≤ 11.0
11.0 – 16.5
16.5 – 22.0
22.0 – 27.5
27.5 – 33.0
33.0 – 38.5
38.5 – 44.0
44.0 – 49.5
49.5 – 55.0
55.0 – 60.5
60.5 – 66.0
66.0 – 71.5
71.5 – 77.0
≥ 77.0
> 77.0
Diameter [µm]
Diameter [µm]

Figure 4

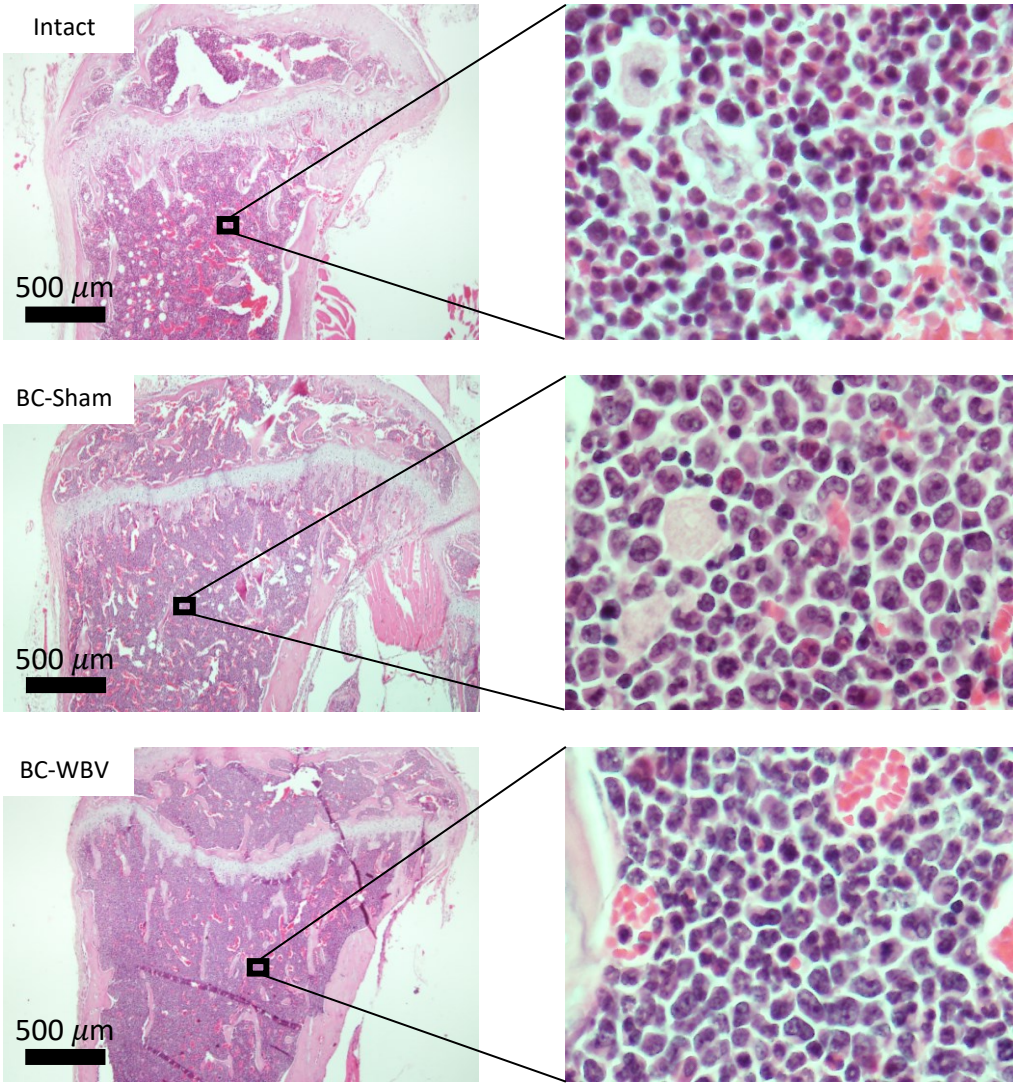

Figure 5